Acta Mech 235, 5937–5946 (2024)
https://doi.org/10.1007/s00707-024-04012-y

Check for updates

NOTE

Franz G. Rammerstorfer

A note on structural mode transitions in buckling of radially stretched annular plates

Received: 6 March 2024 / Revised: 14 May 2024 / Accepted: 21 June 2024 / Published online: 12 July 2024
© The Author(s) 2024

Abstract The different approximating assumptions used in deriving models for structural analysis by dimensional reduction of a 3d continuum to structural components like beams and plates or shells limit the applicability of these models by geometrical constraints. Hence, caution should be exercised when transitioning from the application range of one type of structure model to another one. This should be taken into account especially when stability analyses are performed. In order to demonstrate this, in this note, buckling of annular plates under tensile loading at the inner edge is treated as an example. The ratio between inner and outer radius is varied. For ratios approaching 1.0, plate buckling turns into buckling of circular beams. This is not only a question of accuracy of the solution but can lead to a substantial qualitative change of the character of buckling. Such considerations might be interesting from a theoretical point of view; in any case they are important from the engineering point of view.

1 Introduction

In structural mechanics, the dimensional reduction of a 3d continuum to beam, plate or shell models is performed by applying a number of (kinematic) approximating assumptions. Most common are the reductions to Euler-Bernoulli beam and to Kirchhoff plate or shell models. The applicability of such models in structural analysis is limited by geometrical constraints. For instance, for bending of beams the Poisson effect is treated in a different way as in bending of plates and shells. Thus, for a beam with rectangular cross section with thickness h, the bending stiffness per unit width, $E\frac{h^3}{12}$ becomes $E\frac{h^3}{12(1-\nu^2)}$ for the plate if the width of the cross section gets larger. Twist and warping of the cross section is treated differently, too. This transformation happens gradually. However, regarding buckling mode shapes and, consequently, buckling loads the transition form plat/shell modes to beam modes my lead to quite abrupt changes.

There are a number of structural components, which exhibit gradual or abrupt qualitative changes of the characteristics of the kind of instability by varying typical parameters. From the engineering point of view, one observes such phenomena for instance, when buckling of axially compressed thin circular cylindrical shells is considered. Depending on characteristic geometrical parameters of the shell, buckling mode transitions appear not only by change of wave numbers but also in its principal character such as plate to shell to beam buckling, see, e.g. [1].

Furthermore, there are many types of thin walled structures, which show such mode switching phenomena under tensile loading. A quite intensively examined example are stretched strips with clamped but axially moving ends, see, e.g., [2].

Abrupt transitions of the character of buckling modes may have not only geometric reasons but also other ones. For instance, in [3–5] buckling of stretch-twisted strips is treated. There, the buckling pattern switches

F. G. Rammerstorfer (✉)
Institute of Lightweight Design and Structural Biomechanics, TU Wien (Vienna University of Technology), Vienna, Austria
E-mail: ra@ilsb.tuwien.ac.at

from different types of waves to completely others (e.g., from waves in longitudinal to waves in transverse direction) at particular critical combinations of stretch and torque. For an overview on buckling of structures under tension see, e.g., [6] and [7].

In the present note, the phenomenon of gradual and – more important – abrupt qualitative changes of the characteristics of the kind of instability of annular plates under radial tension at the inner edge is treated as an example representative for situations in which caution is requested if critical loads are determined solely using buckling coefficient diagrams for plate buckling, as they are common in lightweight design; see, e.g., [8], or if one simply assumes that beam buckling is relevant. Similarly, caution should be exercised in such situations when using diagrams of frequency coefficients in dynamics, as presented, e.g., in [9].

Buckling of annular plates is a classic problem which has been discussed in the literature for a long time, see, e.g., [10]. References, which are more specifically related to the problems considered in tis note, can be found in Coman and Haughton [11,12], where plate buckling and wrinkling of annular plates, stretched by radial displacements at the inner and outer edges, is studied, and in [13], where buckling under radial tractions at both edges, which are movable only in-plane and only translationally, is discussed.

In the present note, the focus is not on treating the plate buckling problem but on the transition from plate to beam buckling. Such transitions are considered for different combinations of boundary conditions at the inner and outer edges and for both follower and directional, i.e. non-follower, loading. Critical load intensities as well as the corresponding buckling modes were determined for plate buckling as well as for beam buckling in dependence of the ratio ρ between inner and outer radius, particularly in the range at which mode transitions must be expected, i.e., for ρ-values close to 1.0.

2 Description of the problem and solution methods

Buckling of tensile loaded thin annular plates of homogeneous, isotropic, linear elastic material is considered. Loading the inner edge of an annular plate by a radially oriented uniformly distributed tensile stress σ, see left picture in Fig. 1, leads (assuming plane stress conditions) to the following axisymmetric stress field:

$$\sigma_{rr} = \sigma \frac{\rho^2}{1-\rho^2}\left[\left(\frac{r_a}{r}\right)^2 - 1\right] \text{ and } \sigma_{\varphi\varphi} = -\sigma \frac{\rho^2}{1-\rho^2}\left[\left(\frac{r_a}{r}\right)^2 + 1\right]. \tag{1}$$

Because of the circumferential compression stresses $\sigma_{\varphi\varphi}$ the trivial equilibrium configuration gets unstable, if a critical load intensity $\sigma = \sigma^*$ is reached. This critical load intensity depends, besides others, on the boundary conditions at the inner and outer edge as well as on the ratio $\rho = \frac{r_i}{r_a}$.

In lightweight construction, it is common for plate (and shell) buckling problems to be expressed in non-dimensional form, provided that the structure has a simple geometry (i.e., the geometry is described by a few parameters only). A dimensionless "buckling coefficient" (also called "buckling factor") is introduced either by intuition or by applying dimensional analysis [14].

For buckling of annular plates as studied in this note, such a buckling factor reads

$$k = \frac{\sigma^*}{E}\left(\frac{r_a}{h}\right)^2. \tag{2}$$

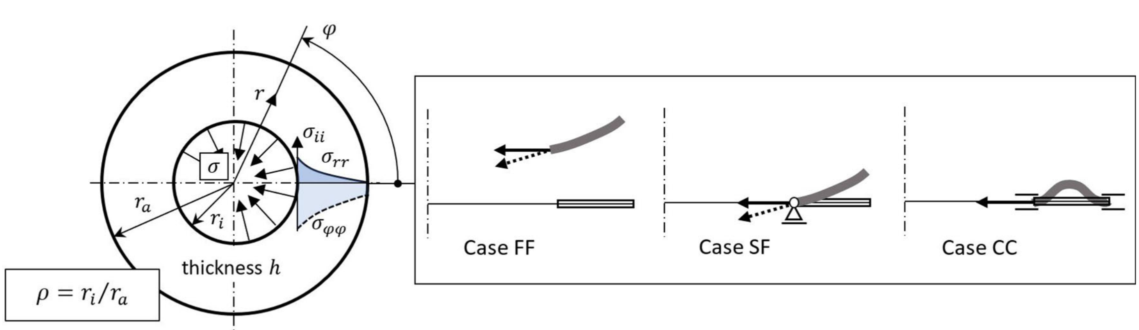

Fig. 1 The tension loaded annular plate - notations (left); definition of boundary conditions for the considered cases (right)

As long as this instability can be characterized as plate buckling, i.e. before mode transition to beam buckling occurs, this buckling factor depends, for given boundary conditions, only on ρ, and the critical stress can be expressed by

$$\sigma^* = kE\left(\frac{h}{r_a}\right)^2. \tag{3}$$

Since the bucking factor k is independent of the actual values of the geometric parameters and of the Young's modulus E it can be determined by calculating the critical load intensity σ^* for a single set of arbitrarily (however sensfully) chosen values of h, r_a, E, and ν and given boundary conditions as a function of sufficiently densely varied values of ρ, regardless of the methods used to carry out these calculations.

In the present note, $k(\rho)$ is determined from $\sigma^*(\rho)$, taken from [15] and [16], having been computed by finite element analyses. Although the buckling problem is not in the focus of this note, the procedure for solving it should be described very briefly: As quite common for long in computational mechanics, the critical load intensity is calculated from the lowest eigenvalue λ_1 of the linear eigenvalue problem $(K_0 + \lambda(K_u + K_g(+K_L)))\Phi = 0$, multiplied by the chosen nominal load intensity. K_0 is the stiffness matrix of the unloaded discretized system. K_u and K_g are the initial displacement and the initial stress (or geometry) matrix, respectively, and K_L is the load stiffness matrix, added in case of follower loading, all at the given nominal load intensity. Φ_i is the eigenvector, representative for the i^{th} eigenmode, corresponding to the i^{th} buckling mode. The continuous i^{th} buckling mode results from Φ_i (describing the mode pointwise) by using the interpolation functions of the elements.

Remark 1 As shown later in this note, plate buckling transitions into beam buckling with increasing values of ρ. Under certain conditions, this happens long before ρ approaches 1.0. When this occurs, Eqs. (2) and (3) may no longer be used from then on.

Examination of the transition from plate to beam bucking is performed for plates with following combinations of boundary conditions (see also Fig. 1, right):

- Case FF: completely free disk; loading character (directional or follower) is relevant, 3d and 2d beam buckling modes are possible.
- Case SF: inner edge simply supported, outer edge free, both edges moveable in the plane only; loading character could be considered relevant for plate buckling; for beam buckling loading character is relevant, only 2d beam buckling mode possible.
- Case CC: both inner and outer edge clamped and moveable in the plane only; loading character is irrelevant for plate buckling; for beam buckling loading character is relevant, only 2d beam buckling mode possible.

Further combinations of boundary conditions are considered in [15].

Remark 2 Note that even if the loading character (directional or follower load) is irrelevant for plate buckling, in all cases considered, for beam buckling—and, hence, for the transition from plate to beam buckling—a distinction must be made between directional and follower loading.

Knowing $k(\rho)$, the critical radial tensile stress at the inner edge of any thin annular plate, i.e. $h << r_a$ made of linear elastic, isotropic material, can be determined quite easily for any set of values of the parameters h, r_a, E, by using Eq. (3). However, as ρ approaches 1.0, the annular plate is more likely to behave as a circular beam with rectangular cross section ($b \times h$), with $b = r_a - r_i = r_a(1-\rho)$. Since Eqs. (3) and (2) are applicable only as long as plate buckling can be assured, it is important to know the limit of $\rho = \rho*$, above which these equations are no longer valid and beam buckling must be considered.

The transformation from plate model to beam model happens gradually. This means that conditions assumed for describing plate behavior change gradually to those for describing beam behavior. For instance, in the Bernoulli-Euler beam formulation following differences appear in comparison with the Kirchhoff plate formulation:

- The external load, i.e., the tensile stress σ at the inner edge of the annular structure must be transformed to $\bar{\sigma} = \sigma\frac{1+\rho}{2}$, leading to the distributed radial load per unit length $q = \bar{\sigma}h$, acting along the beam axis.
- The circumferential stress is assumed to be constant along the width b with $\bar{\sigma}_{\varphi\varphi} = \frac{\bar{\sigma}r_m}{b} = \sigma\frac{(1+\rho)^2}{4}\frac{r_a}{b}$.
- Compared to the circumferential stress $\bar{\sigma}_{\varphi\varphi}$ the radial stress σ_{rr} becomes negligibly small and, thus, is disregarded.

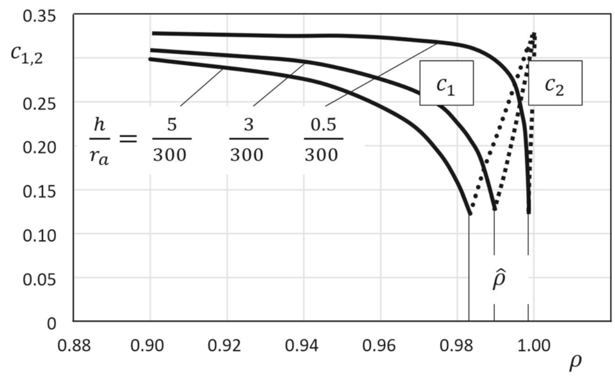

Fig. 2 Factor c for torsional stiffness of not sufficiently slim rectangular cross sections, i.e., if l not much larger than t

- The influence of the Poisson's ratio ν on the bending stiffness, which for plates is given by $\frac{1}{1-\nu^2}$, disappears completely.
- Torsional stiffness effects come into account with the torsional stiffness GJ_T, where the Poisson's ratio plays a role in the relation $G = \frac{E}{2(1+\nu)}$.

For rectangular cross sections with one edge significantly longer than the other, J_T is approximated by $J_T = lt^3/3$ with l being the longer edge of the cross section and t the short one. However, the more square the cross section becomes, the more this approximation fails, and according to [17], J_T has to be calculated by

$$J_T = c\, l\, t^3 \text{ with } \mathrm{c} = \frac{1}{3}\left[1 - \frac{0.63}{\mathrm{t/l}} + \frac{0.053}{(\mathrm{t/l})^5}\right]. \tag{4}$$

It is important to note that the quantities l and t in Eq. (4) change their meaning when ρ gets larger than $\hat{\rho}$, with $\hat{\rho} = 1 - \frac{h}{r_a}$.

This means that for $\rho \leq \hat{\rho}$, one has to use $l = b$ and $t = h$, leading to $c = c_1$, and for $\hat{\rho} < \rho < 1.0$ one has to chose $l = h$ and $t = b$, resulting in $c = c_2$; see Fig. 2, which shows the dependence of the factor c, used in Eq. (4), on ρ for several ratios h/r_a.

Circular beams, radially stretched at r_i, are prone to buckle either out-of-plane (3d modes) or in-plane (2d modes). It should be noted that for circular beams the critical tensile stress σ^* depends in all considered cases on the load character, i.e., if directional or follower load is applied. Furthermore, as long as plate buckling is concerned, the dimensionless buckling factor, Eq. (2), depends only on ρ. However, if a buckling factor should be used as in Eq. (3) also for beam buckling, then its dependence on the ratio h/r_a must be considered, too.

With the above mentioned conditions for the plate to beam transition, the following expressions for the buckling factors for beam buckling are derived:

(a) *3d mode under directional tensile loading*

The 3d beam buckling mode, also called twist mode, is relevant for Case FF only. Starting with the critical line load, acting in radial direction along the beam axis, as given in [18]:

$$q_{3d}^* = \bar{\sigma}_{3d}^* h = \frac{9EJ_{rr}}{\left(4 + \frac{EJ_{rr}}{GJ_T}\right) r_m^3}. \tag{5}$$

Some algebraic manipulation and taking into account that in the considered case the tensile load acts at the inner edge, one obtains the buckling factor for 3d beam buckling as

$$\bar{k}_{3d} = \frac{12(1-\rho)}{(4+\kappa)(1+\rho)^4}. \tag{6}$$

The quantity κ is given by

$$\kappa = \frac{1+\nu}{6c_1} \text{ for } \rho \leq \hat{\rho} \text{ and } \kappa = \frac{1+\nu}{6c_2}\left[\frac{h}{r_a(1-\rho)}\right]^2 \text{ for } \rho > \hat{\rho}. \tag{7}$$

There, c_1 is determined as c with $t = h$ and $l = b$; for c_2 the quantity c is calculated with $t = b$ and $l = h$.

(b) *3d mode under follower tensile loading*
Based on the solution as presented in [18], the buckling factor for 3d beam buckling under follower loading is derived as $\bar{k}^f_{3d} = \frac{3}{4}\bar{k}_{3d}$.

(c) *2d mode under directional tensile loading*
In Case FF the transition from plate to beam buckling leads first to the 3d beam mode (twist mode) when ρ approaches 1.0. In Cases SF and CC, 3d beam buckling is not possible, and the plate to beam transition leads directly to a 2d beam mode.
Again, starting with a solution taken from [18] for 2d beam buckling under the critical line load acting in radial direction along the beam axis,

$$q^*_{2d} = \bar{\sigma}^*_{2d} h = 4\frac{EJ_{rr}}{r_m^3}, \tag{8}$$

after some algebraic manipulation one gets

$$\bar{k}_{2d} = \frac{16(1-\rho)^3}{3(1+\rho)^4}\left(\frac{r_a}{h}\right)^2. \tag{9}$$

(d) *2d mode under follower tensile loading*
Based on the solution as presented in [18], the buckling factor for the 2d beam mode for follower loading is derived as

$$\bar{k}_{2d} = \frac{12(1-\rho)^3}{3(1+\rho)^4}\left(\frac{r_a}{h}\right)^2. \tag{10}$$

In contrast to plate and 3d beam buckling, for 2d beam modes the influence of the Poisson's ratio on the buckling factor is not present.

3 Results and discussion

The primary objective of this paper is to examine the transitions from plate to beam buckling, which typically occurs at values of ρ close to 1.0. Nevertheless, this section also provides an overview of the buckling behavior of stretched annular plates under various boundary conditions for $\rho \in [0.4, 1.0]$. The shown diagrams are valid for $\nu = 0.3$.

3.1 Plate buckling

As described in the previous section, one has to distinguish between areas of ρ in which plate models and areas in which beam models, respectively, should be used.

Let us first consider the dependence of the plate buckling factor on the radius ratio ρ, regardless of the limitation of the applicability of the plate model—see Fig. 3.

As is shown in this figure, for the transition from plate to beam buckling (region of specific interest) follower load effects are relevant in Case FF already for plate buckling. In contrast, in Case SF, follower load effects are not present in the considered region of ρ. In Case CC, *per se* no follower load effect appears as long as plate buckling is concerned.

Note that in Case FF the wave number remains $n = 2$ for all considered ratios ρ. For the other boundary conditions, i.e., Cases SF and CC, one observes $n(\rho)$ values, which grow stepwise with increasing ρ and become quite large for ρ approaching 1.0. However, one should bear in mind, that for regions of ρ close to 1.0 (region of specific interest), plate buckling may no longer be relevant and beam buckling may occur.

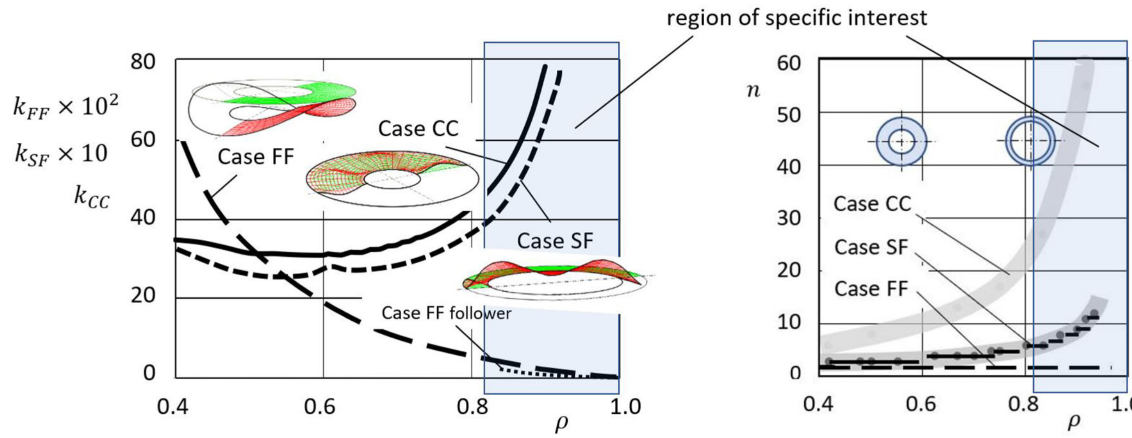

Fig. 3 Dependence of the buckling factor k (left image) and of the buckling wave number n (right image) on the radius ratio ρ for the considered cases. Restrictions on the validity of the plate buckling (in the "region of specific interest") have not yet been taken into account in this figure. The data used comes partly from [15] and partly from [16]

4 Transition from plate to beam buckling

In Fig. 4, the k-values calculated for Case FF with the plate, 3d beam, and 2d beam models are shown in their dependence of ρ within the "region of specific interest". There, the ratio h/r_a is chosen as $1/300$, as an example.

One observes that with increasing ρ in the "region of specific interest" first plate buckling turns more and more into beam buckling, and when the k_{FF}-curves for 3d and 2d beam buckling cross each other (at $\rho = \rho^*$), 3d beam buckling abruptly changes to 2d beam buckling. The gradual transition from plate to 3d beam buckling is, as mentioned above, caused by the gradual change of the validity of the conditions assumed for describing plate behavior to those for describing beam behavior with increasing ρ.

It is usually assumed that the smallest eigenvalue should be used to determine the buckling load. This assumption applies in any case to the change from 3d to 2d beam buckling (right image in Fig. 4). However, the area before the transition from plate to beam buckling begins (left area in the left image of Fig. 4) shows something different. There, the k-values calculated with the beam model are smaller than those calculated with the plate model, but are no longer correct and, hence, those determined with the plate model apply although they are larger.

Remark 3 The assumption that the smallest of the calculated buckling loads is decisive as long as one and the same analysis model is used in the respective stability analysis. However, if different models based on different

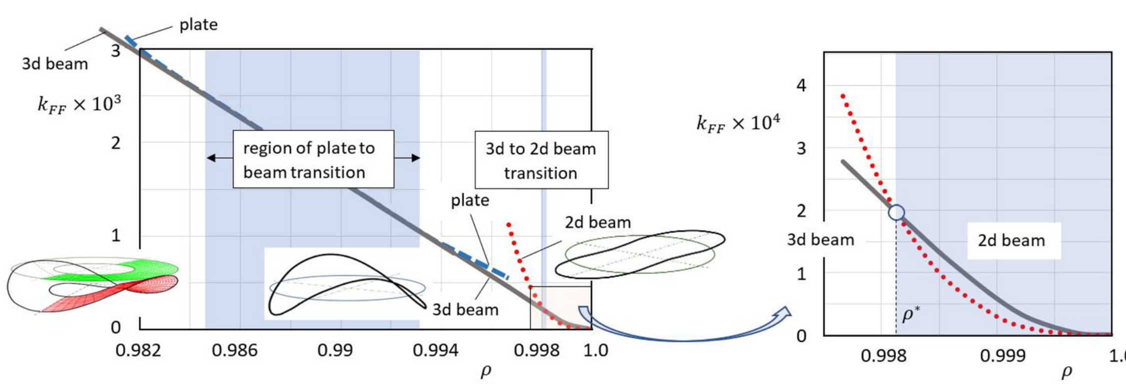

Fig. 4 Case FF—Left image: buckling factor for plate, 3d beam, and 2d beam buckling, dependent on ρ within the "region of specific interest"; $h/r_a = 1/300$, directional loading. For follower loading, the values at the ordinate correspond to $\frac{4}{3}k^f_{FF} \times 10^3$. Right image: Detail of left image for ρ-values, where 3d to 2d beam buckling occurs. For follower loading, the values at the ordinate correspond to $\frac{4}{3}k^f_{FF} \times 10^4$

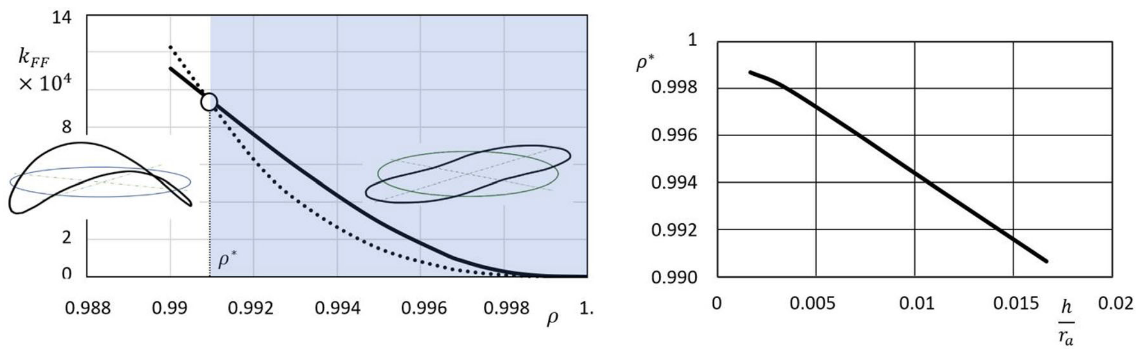

Fig. 5 Case FF – Left image: Transition from 3d to 2d buckling for $h/r_a = 5/300$; directional loading. For follower loading the values at the ordinate correspond to $\frac{4}{3}k^f_{FF} \times 10^4$. Right image: ρ^* as a function of $\frac{h}{r_a}$; valid for both directional and follower loading

approximations are used, it may easily be that the smallest of the buckling loads calculated by the different models is less correct than the larger one.

The left image in Fig. 5 shows the transition from 3d to 2d beam bucking for a value of the ratio $h/r_a = 5/300$, i.e. for a relatively thick plate, as an example for comparison. At first glance this image looks pretty much the same as the right image in Fig. 4. However, notice the scaling of the axes! The value of ρ^*, at which the 3d to 2d transition occurs, depends on the ratio h/r_a.

Using Eqs. (6) and (9), the following implicit nonlinear relation for ρ^* is found:

$$1 - \rho^* - \frac{3}{2\sqrt{4 + \kappa\left(\frac{h}{r_a}, \rho = \rho^*\right)}} \frac{h}{r_a} = 0 \tag{11}$$

with $\kappa\left(\frac{h}{r_a}, \rho\right)$ according to Eq. (7). Eq. (11) is valid for both directional and follower loading. Solutions of Eq. (11) are depicted in Fig. 5 (right image).

As mentioned above, in Case FF the wave number for all buckling modes is always $n = 2$. However, in Cases SF and CC the wave number grows rapidly as ρ approaches the value 1.0; see Fig. 3 (right image). Thus, for these cases no simple relation for ρ^* as function of h/r_a can be provided.

Figure 6 shows the mode transition from plate to 2d beam buckling for Case SF (left figure) and for the Case CC (right figure). Both directional and follower loading is considered.

While in Case FF the transition from plate to beam buckling happens at values of ρ, which are very close to 1.0, for the other cases this transition appears at significantly lower ρ-values.

Remark 4 Approaches for determining the critical tension σ^*, which allow only solutions of the form $w(r, \varphi) = W(r)\sin(n\varphi)$ for the out-of-plane displacement w and, hence, buckling factor diagrams derived from them don't capture the transition from 3d to 2d buckling. Therefore, caution should be exercised in buckling analyses of plate like structures if geometries are envolved that tend to be represented by beam models rather than by

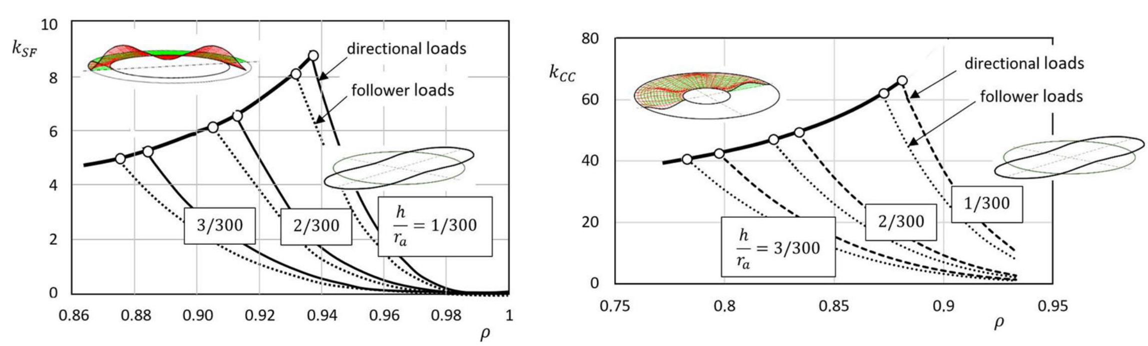

Fig. 6 Transition from plate to 2d beam buckling for different ratios h/r_a. Left image: Case SF; right: Case CC

plate models. In such situations using plate buckling factor diagrams alone can lead to results, that are unsuitable for determining buckling resistance.

5 Conclusions

When considering thin walled structures in terms of structural mechanics, typically beam, plate, and shell models are applied. In these models, a number of assumptions are used for the reduction from a 3d continuum to a 2d (shell, plate) structure, and even more approximating assumptions are accepted for achieving 1d (beam) models. Because of the differences in these assumptions, one has to take care, when there is a situation, in which—due to geometrical relations—a shell or a plate becomes rather a beam. In this note, buckling of annular plates, which are stretched by tensile forces at the inner edge, is studied as an example for such a structural transformation.

In general, the transformation from shell/plate to beam happens gradually. However, it is important to note that abrupt transitions of buckling modes may appear in geometrical relations, for which just one of the two model approximations, i.e., either shell/plate or beam, is able to describe the modes in a sufficiently correct way. Such abrupt mode transitions are investigated in the present paper.

From the engineering point of view, the following warning should be considered: Caution must be exercised when using the most convenient plate buckling factor k for plate buckling only. One should be aware of the fact that its application is limited by possible mode switching from plate to beam buckling, which is determined by geometrical parameters and boundary as well as loading conditions.

Some case studies are presented in the Appendix to underline the focus of this note.

Open Access This article is licensed under a Creative Commons Attribution 4.0 International License, which permits use, sharing, adaptation, distribution and reproduction in any medium or format, as long as you give appropriate credit to the original author(s) and the source, provide a link to the Creative Commons licence, and indicate if changes were made. The images or other third party material in this article are included in the article's Creative Commons licence, unless indicated otherwise in a credit line to the material. If material is not included in the article's Creative Commons licence and your intended use is not permitted by statutory regulation or exceeds the permitted use, you will need to obtain permission directly from the copyright holder. To view a copy of this licence, visit http://creativecommons.org/licenses/by/4.0/.

Funding Open access funding provided by TU Wien (TUW).

Appendix

In order to express the main intention for writing this note, in this Appendix a few case studies are presented by numerical examples.

Let as first consider a situation, in which the plate (3d) to beam (2d) transition of the buckling mode has severe consequences with respect to the critical load intensity σ^*. For this purpose two annular membranes (treated as plates), made of Mylar, are examined with both inner and outer edges clamped but movable in the plane, i.e., **Case CC**.

CC Plate I: $r_a = 5\,\text{mm}$, $r_i = 4\,\text{mm}$, $h = 0.0333\,\text{mm}$, $E = 2.8 \times 10^3\,\text{MPa}$; load character: follower. This data leads to $\rho = 0.8$, $h/r_a = 0.00667$.

Using the left diagram in Fig. 7, one gets k for plate buckling, i.e, 3d buckling as $k = 43$, resulting with Eq. (3) in $\sigma^* = 5.35\,\text{MPa}$. For 2d beam buckling, k is determined by Eq. (10) as $k = 69$, what with Eq. (3) gives: $\sigma^* = 8.59\,\text{MPa}$.

Comparing the results for plate and beam buckling shows that in this case plate buckling is the relevant mode. (Note that in Case CC, because of the boundary conditions, 3d beam buckling is not possible.)

CC Plate II: Same data as for CC Plate I, except the value of r_i which is now a bit larger, namely $r_i = 4.25$ mm. With this data, the radius ratio is $\rho = 0.85$, and one gets for plate buckling $k = 54$ leading to $\sigma^* = 6.72$ MPa; for beam buckling, $k = 26$ results in $\sigma^* = 3.23$ MPa. Thus, in this case 2d, i.e., beam buckling is the relevant mode. If only the $k(\rho)$ diagram (Fig. 7, left) had been used for plate buckling, the critical load intensity for CC Plate II would have been overestimated by more than 100%!

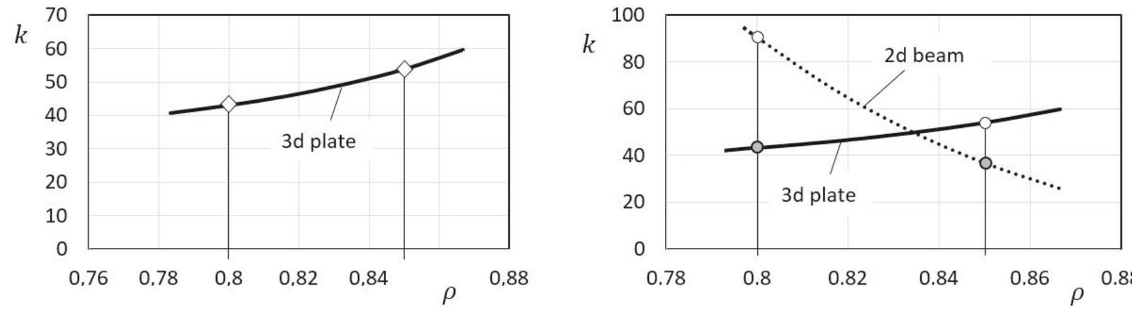

Fig. 7 Buckling factors for CASE CC; left: plate buckling factor (cut-out from Fig. 3); right: buckling factors for both, 3d plate buckling (full line) and 2d beam buckling (dotted line)

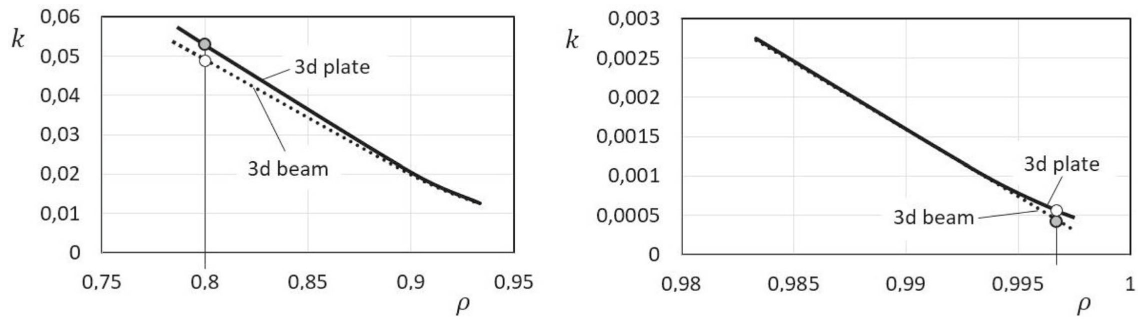

Fig. 8 Buckling factors for Case FF (cut-outs from Fig. 4); full lines: 3d plate buckling; dotted lines: 3d beam buckling

In the right diagram in Fig. 7, the relevant critical load intensities are indicated be filled circle symbols, and the not relevant, i.e., the (in view of practical use) misleading values are indicated by empty circle symbols.

The transition from 3d plate to 3d beam buckling, treated in the following examples of completely free annular plates (**Case FF**) made of steel, is gradual and, thus, less dramatic but still interesting.

FF Plate I: $r_a = 250\,\text{mm}$, $r_i = 200\,\text{mm}$, $h = 0.833\,\text{mm}$, $E = 2.1 \times 10^5$ MPa; load character: directional. This data leads to $\rho = 0.8$, $h/r_a = 0.00333$.

Using Fig. 8, left, one gets for plate buckling (full line) $k = 0.053$, resulting with Eq. (3) in $\sigma^* = 0.124$ MPa, and the buckling factor for 3d beam buckling is determined either from Fig. 8, left (dotted line), or by applying Eqs. (4) to (7) as $k = 0.049$, leading to $\sigma^* = 0.114$ MPa.

Note: Although normally the lower value of critical load intensity is relevant, in this case plate buckling with the larger critical load is the correct mode. The reason for this unusual decision is that for decreasing values of ρ the beam model loses its validity and the plate model describes reality better.

FF Plate II: Same data as for FF Plate I, except the value of r_i which is now larger, namely $r_i = 249.2\,\text{mm}$ and, correspondingly, $\rho = 0.997$. From Fig. 8, right, one gets for plate buckling $k = 0.00057$ and, hence, $\sigma^* = 0.133$ kPa. The buckling factor for 3d beam buckling is $k = 0.000454$ and $\sigma^* = 0.088$ kPa. Here, the structure is no longer a plate, but clearly a beam, and 3d beam buckling with the smaller value of σ^* is relevant.

In both cases, FF Plate I and FF Plate II, 2d beam buckling does not need to be taken into account, see Fig. 4. A transition from 3d beam buckling to 2d beam buckling could be discussed for values of ρ extremely close to 1, see Figs. 4 and 5.

References

1. Todt, M., Rammerstorfer, F.G.: Analytical Stability Considerations in Lightweight Design. In: Altenbach, H., Öchsner, A. (eds.) Encyclopedia of Continuum Mechanics. Springer, Berlin, Heidelberg (2018) . (ISBN: 978-3-662-53605-6)
2. Rammerstorfer, F.G.: Buckling of stretched strips - reconsidered and extended. Comput. Struct. (2024). https://doi.org/10.1016/j.compstruc.2023.107193
3. Chopin, J., Demer, V., Davidovitch, B.: Roadmap to the morphological instabilities of a stretched twisted ribbon. J. Elast. **119**, 137–189 (2015). https://doi.org/10.1007/s10659-014-9498-x
4. Kudrolli, A., Chopin, J.: Tension-dependent transverse buckles and wrinkles in twisted elastic sheets. Proc. R. Soc. A. (2018). https://doi.org/10.1098/rspa.2018.0062
5. Faghfouri, S., Rammerstorfer, F.G.: Mode transitions in buckling and post-buckling of stretched-twisted strips. J. Non-Linear Mech. **127**, 103609 (2020). https://doi.org/10.1016/j.ijnonlinmec.2020.103609
6. Rammerstorfer, F.G.: Buckling of elastic structures under tensile loads. Acta Mech. **229**, 881–900 (2018). https://doi.org/10.1007/s00707-017-2006-1
7. Wang, T., Yang, Y., Xu, F.: Mechanics of tension-induced film wrinkling and restabilization: a review. Proc. Royal Society A, Issue **226327**, 20220149 (2022). https://doi.org/10.1098/rspa.2022.0149
8. Megson, T.H.G.: Aircraft structures, Arnold, 3rd edn, p. 172 (1999). ISBN 0 340 70588 4
9. Leissa, A.: Vibration of plates, NASA SP-160, National Aeronautics an Space Administration, Washington D.C. (1969). ISBN 0 340 70588 4
10. Bloom, F., Coffin, D.: Handbook of thin plate buckling and postbuckling. Chapman and Hall/CRC, UK (2001)
11. Coman, C.D., Haughton, D.M.: Localized wrinkling instabilities in radially stretched annular thin films. Acta Mech. **185**, 179–200 (2006). https://doi.org/10.1007/s00707-005-0307-2
12. Coman, C.D.: On the applicability of tension field theory to a wrinkling instability problem. Acta Mech. **190**, 57–92 (2007). https://doi.org/10.1007/s00707-006-0395-7
13. Coman, C.D., Haughton, D.M.: On some approximate methods for the tensile instabilities of thin annular plates. J. Eng. Math. **56**, 79–99 (2006). https://doi.org/10.1007/s10665-006-9041-6
14. Gibbings, J.C.: Dimensional analysis. Springer-Verlag, Berlin (2011). (ISBN 978-1-84996-316-9)
15. Rammerstorfer, F.G.: Buckling of annular plates under tensile loading - plate to beam ransitions, ILSB Report No 308-red, internal report at the Inst. Lightweight Design and Struct. Biomech., TU Wien (2024)
16. Herk, D.: Instabilitaeten bei gelochten Kreisplatten unter radialer Zugbelastung am Innenrand. Diplomarbeit, ILSB, TU Wien (2021)
17. Young, W.C., Budynas, R.G.: Roark's formulas for stress and strain, McGraw-Hill Education (2001). ISBN 10: 007072542X / ISBN 13: 9780070725423
18. Pflüger, A.: Stabilitaetsprobleme der Elastostatik. Springer, Berlin Heidelberg (1964). https://doi.org/10.1007/978-3-662-25023-5-4

Publisher's Note Springer Nature remains neutral with regard to jurisdictional claims in published maps and institutional affiliations.